Spatiotemporal control of high-intensity laser pulses with a plasma lens

D. Li [1,*] K. G. Miller [2] J. R. Pierce,[3] W. B. Mori,[3] A. G. R. Thomas,[1] and J. P. Palastro [2,†]

[1]*Gérard Mourou Center for Ultrafast Optical Science, University of Michigan, Ann Arbor, Michigan 48109, USA*

[2]*University of Rochester, Laboratory for Laser Energetics, Rochester, New York 14623-1299, USA*

[3]*Department of Physics and Astronomy, University of California, Los Angeles, California 90095, USA*

(Received 19 December 2023; accepted 12 February 2024; published 12 March 2024)

Spatiotemporal control encompasses a variety of techniques for producing laser pulses with dynamic intensity peaks that move independently of the group velocity. This controlled motion of the intensity peak offers a new approach to optimizing laser-based applications and enhancing signatures of fundamental phenomena. Here, we demonstrate spatiotemporal control with a plasma optic. A chirped laser pulse focused by a plasma lens exhibits a moving focal point, or "flying focus," that can travel at an arbitrary, predetermined velocity. Unlike currently used conventional or adaptive optics, a plasma lens can be located close to the interaction region and can operate at an orders of magnitude higher, near-relativistic intensity.

DOI: 10.1103/PhysRevResearch.6.013272

I. INTRODUCTION

Spatiotemporal pulse shaping uses advanced optical techniques to construct laser pulses with dynamic and controllable properties [1–18]. The laser pulses created with these techniques can exhibit an intensity peak that travels faster than the speed of light [3,4], accelerates [16,17], or even oscillates [3,17], all while maintaining a near-constant profile over distances far greater than a Rayleigh range. The flexibility to control the motion of the peak intensity has provided new opportunities to optimize laser-based applications and enhance signatures of fundamental phenomena [8,10,19–26]. Nevertheless, many of these opportunities require intensities that would damage the conventional and adaptive optics used to structure the laser pulse.

Plasma optics, having been ionized, can withstand orders of magnitude higher intensities than conventional or adaptive optics [27–44]. The refractive index in a plasma depends on the electron density and the frequency of the laser pulse. As a result, spatial variation, temporal evolution, or nonlinearity in the electron density can be used to reflect [31,32], refract [30,33,35], diffract [38,41,44], disperse, frequency convert [42,45,46], or amplify laser pulses [28,29,40]. In fact, several experiments already make routine use of plasma optics based on these processes: plasma gratings tune the symmetry of implosions at the National Ignition Facility [47,48], plasma waveguides extend the interaction lengths in laser wakefield accelerators [49,50], and plasma mirrors enhance the intensity contrast in ultrashort pulse lasers [31,32].

Here, we demonstrate that a plasma optic can be used for the spatiotemporal control of high-intensity laser pulses. A preformed plasma channel functions as a thick, chromatic lens that focuses different frequencies in a laser pulse to different locations along the propagation axis. The chirp of the laser pulse determines the arrival time of the frequencies at these locations. The time-dependent focusing of the pulse produces a moving focal point with an arbitrary velocity that can be tuned by adjusting the chirp (Fig. 1). This configuration is a plasma-based version of the original chromatic flying focus [4], which has been proposed for a range of experiments, including Raman amplification [19], photon acceleration [21,51], nonlinear Thomson scattering [23], and vacuum birefringence [52]. However, unlike the diffractive optic used in the original flying focus, a plasma lens can be

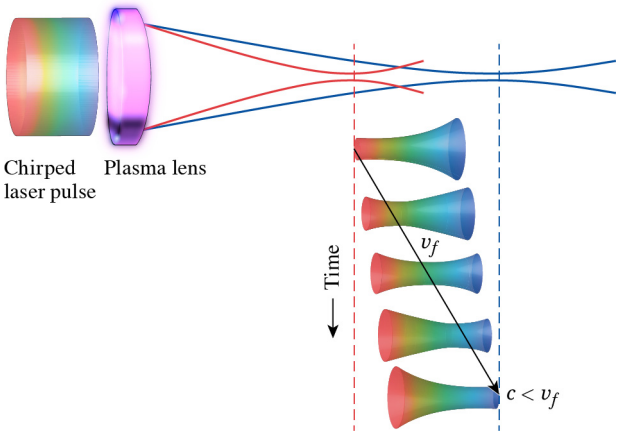

FIG. 1. A chirped laser pulse focused by a plasma lens results in a moving, or "flying," focus with an intensity peak that moves independently of the group velocity. The plasma lens focuses different frequencies to different longitudinal locations, while the chirp controls the arrival time of the frequencies at these locations. In this case, the velocity of the moving focus is superluminal ($v_f > c$).

*dionli@umich.edu
†jpal@lle.rochester.edu

placed close to the interaction region and can operate at an orders of magnitude higher, near-relativistic intensity.

The remainder of this article begins with a model for the propagation of a laser pulse focused (or guided) by a plasma lens (Sec. II). The model is general enough to describe the focusing of arbitrary, space-time-structured laser pulses, with or without orbital angular momentum. The model predicts that the chromatic aberration of the plasma lens and the chirp of a laser pulse can be used to produce an intensity peak with a specified constant velocity (Sec. III). The plasma lens is designed to produce an extended focal region, while avoiding resonance absorption and mitigating parametric instabilities (Sec. IV). Particle-in-cell simulations based on this design validate the model for moderate intensities and determine the intensities and durations at which the plasma lens ceases to operate as expected (Sec. V). The article concludes with a summary of the results and a discussion of future prospects (Sec. VI).

II. PLASMA LENS

Consider a linearly polarized laser pulse propagating in the positive $\hat{\mathbf{z}}$ direction. The pulse is normally incident on a preformed plasma channel with an entrance and exit located at $z = 0$ and $z = L_p$, respectively. The transverse electric field of the pulse can be expressed as a superposition of its frequency components:

$$E(\mathbf{x}, \xi) = \frac{1}{4\pi} \int e^{-i\omega\xi} \tilde{E}(\mathbf{x}, \omega) d\omega + \text{c.c.}, \tag{1}$$

where $\xi = t - z/c$ is the moving-frame coordinate. At the entrance to the channel, the transverse profile of each component is given by

$$\tilde{E}(\mathbf{x}_\perp, z = 0, \omega) = \sum_{q,\ell} \alpha_{q,\ell} A_I \left(\frac{\sqrt{2}r}{w_I}\right)^{|\ell|} L_q^{|\ell|}\left(\frac{2r^2}{w_I^2}\right) \times \exp\left[-\frac{r^2}{w_I^2} + \frac{i\omega r^2}{2cR_I} + i\ell\theta + i\phi_I\right], \tag{2}$$

where $r = (x^2 + y^2)^{1/2}$, θ is the azimuth, $L_q^{|\ell|}$ is a generalized Laguerre polynomial with radial and orbital angular momentum mode numbers q and ℓ, and $\alpha_{q,\ell}$ quantifies the projection of each mode onto the initial profile. The incident amplitude A_I, phase ϕ_I, spot size w_I, and radius of curvature R_I may all depend on frequency.

Each frequency component of the pulse will refract from the plasma, advance in phase, and diffract by a different amount. This frequency-dependent evolution is described by the paraxial wave equation

$$\left(2i\omega\frac{\partial}{\partial z} + c\nabla_\perp^2\right)\tilde{E}(\mathbf{x}, \omega) = \frac{1}{c}\omega_p^2(\mathbf{x})\tilde{E}(\mathbf{x}, \omega), \tag{3}$$

where $\omega_p^2(\mathbf{x}) = e^2 n(\mathbf{x})/m_e\varepsilon_0$ is the square of the plasma frequency and $n(\mathbf{x})$ is the electron density. Here, the plasma response is assumed to be linear, such that $n(\mathbf{x})$ is independent of E (see Sec. V for particle-in-cell simulations that include nonlinear effects). The plasma channel is modeled using a parabolic density profile

$$n(\mathbf{x}) = n_0 + \tfrac{1}{2}n_2 r^2 \tag{4}$$

for $0 \leqslant z \leqslant L_p$, and $n(\mathbf{x}) = 0$ otherwise. With this profile, the refractive index in the plasma, $\mu(\mathbf{x}, \omega) = [1 - \omega_p^2(\mathbf{x})/\omega^2]^{1/2}$, has an on-axis maximum, which bends the "rays" of the pulse towards the optical axis ($r = 0$) like a lens.

The transverse profile of each frequency component at any $z > 0$ can be found by solving the paraxial wave equation with the initial condition in Eq. (2). The solution is

$$\tilde{E}(\mathbf{x}, \omega) = \sum_{q,\ell} \alpha_{q,\ell} A(z) \left[\frac{\sqrt{2}r}{w(z)}\right]^{|\ell|} L_q^{|\ell|}\left[\frac{2r^2}{w^2(z)}\right] \times \exp\left[-\frac{r^2}{w(z)^2} + \frac{i\omega r^2}{2cR(z)} + i\ell\theta + i\phi^{q,\ell}(z)\right]. \tag{5}$$

Within the plasma channel ($0 \leqslant z \leqslant L_p$), the frequency-dependent amplitude, phase, spot size, and radius of curvature are given by

$$A(z) = \frac{w_I}{w(z)} A_I, \tag{6}$$

$$\phi^{q,\ell}(z) = \phi_I - \frac{\omega_{p0}^2}{2c\omega} z - (2q + |\ell| + 1)\text{atan}\left[\frac{w_I^2 Z_m}{w_m^2 R_I} + \left(\frac{w_m^2}{w_I^2} + \frac{w_I^2 Z_m^2}{w_m^2 R_I^2}\right)\tan\left(\frac{z}{Z_m}\right)\right], \tag{7}$$

$$w(z) = w_I\left[1 + \frac{Z_m}{R_I}\sin\left(\frac{2z}{Z_m}\right) + \left(\frac{Z_m^2}{R_I^2} + \frac{w_m^4}{w_I^4} - 1\right)\sin^2\left(\frac{z}{Z_m}\right)\right]^{1/2}, \tag{8}$$

$$R(z) = R_I \frac{w^2(z)}{w_I^2}\left[\cos\left(\frac{2z}{Z_m}\right) + \frac{R_I}{2Z_m}\left(\frac{Z_m^2}{R_I^2} + \frac{w_m^4}{w_I^4} - 1\right)\sin\left(\frac{2z}{Z_m}\right)\right]^{-1}, \tag{9}$$

where $w_m = (8c^2/\omega_{p2}^2)^{1/4}$ is the "matched" spot size of the plasma channel, $Z_m = \omega w_m^2/2c$ is the Rayleigh range associated with the matched spot size, $\omega_{p0}^2 = e^2 n_0/m_e\varepsilon_0$, and $\omega_{p2}^2 = e^2 n_2/m_e\varepsilon_0$.

After the plasma channel ($z > L_p$), the frequency-dependent amplitude, phase, spot size, and radius of curvature can be expressed in terms of their values at $z = L_p$. Denoting a quantity at the exit of the plasma channel with the subscript l [e.g., $A_l \equiv A(L_p)$], one finds

$$A(z) = \frac{w_l}{w(z)} A_l, \tag{10}$$

$$\phi^{q,\ell}(z) = \phi_l^{q,\ell} - (2q + |\ell| + 1)\text{atan}\left(\frac{z - L_p}{Z_l}\right), \tag{11}$$

$$w(z) = w_l\left[\left(\frac{z-L_p+R_l}{R_l}\right)^2+\left(\frac{z-L_p}{Z_l}\right)^2\right]^{1/2}, \quad (12)$$

$$R(z) = R_l\frac{w^2(z)}{w_l^2}\left[1+\left(1+\frac{R_l^2}{Z_l^2}\right)\left(\frac{z-L_p}{R_l}\right)\right]^{-1}, \quad (13)$$

where $Z_l = \omega w_l^2/2c$. Equations (10)–(13) describe the focusing (or defocusing) of an arbitrary Laguerre-Gaussian mode by a lens with a focal length of

$$f_l = -\frac{R_l}{1+R_l^2/Z_l^2} \quad (14)$$

to a minimum spot size of

$$w_f = \frac{2cf_l}{\omega w_l}\left(\frac{2}{1+\sqrt{1-4f_l^2/Z_l^2}}\right) \quad (15)$$

in the plane $z = L_p + f_l$. Thus, a plasma channel can be used as a lens.

For nearly all parameters of interest, $|R_I| \gg Z_I \gg Z_m$ and $Z_l \gg |R_l|$ (see Appendix A). Under these conditions, the focal length and focused spot size of the plasma lens reduce to the relatively simple expressions

$$f_l(\omega) \approx \frac{\omega w_m^2}{2c}\cot\left(\frac{2cL_p}{\omega w_m^2}\right), \quad (16)$$

$$w_f(\omega) \approx \frac{w_m^2}{w_I}\left|\csc\left(\frac{2cL_p}{\omega w_m^2}\right)\right|, \quad (17)$$

for $j\pi \leqslant L_p/Z_m \leqslant (j+\frac{1}{2})\pi$ and j an integer, which ensures $f_l > 0$. Equation (17) shows that the focused spot size will be smaller than the initial spot size when $w_I > w_m$. When $w_I < w_m$, the spot size initially expands in the lens and then decreases, which ultimately results in $w_f > w_I$. If $L_p \ll Z_m$, the laser pulse does not appreciably diffract or refract within the plasma lens, $w_l \approx w_I$, and Eqs. (16) and (17) further reduce to $f_l(\omega) \approx Z_m^2/L_p$ and $w_f(\omega) \approx 2cf_l/\omega w_l$. This is the "thin" lens limit. Otherwise, the plasma lens is considered "thick." Regardless of the thickness, the focal length of the plasma lens depends on frequency; i.e., the lens is chromatic.

III. PLASMA LENS FLYING FOCUS

The plasma lens focuses each frequency component of the laser pulse to a different longitudinal location $z_f(\omega) = L_p + f_l(\omega)$. This produces an extended focal range with a length determined by the minimum and maximum frequencies:

$$L_f = f_l(\omega_{\max}) - f_l(\omega_{\min}). \quad (18)$$

Each frequency arrives at its focal location at a different time $t_f(\omega)$. The focal time is the sum of two contributions: the relative timing of each frequency within the laser pulse at the exit of the plasma lens, i.e., $\partial_\omega\phi_l^{q,\ell}(\omega)$, and the time it takes each frequency to travel a distance $f_l(\omega)$. In total,

$$t_f(\omega) = \frac{1}{c}f_l(\omega) + \partial_\omega\phi_l^{q,\ell}(\omega). \quad (19)$$

The frequency-dependent focal location and time result in a moving focal point with a velocity of

$$v_f(\omega) = \frac{dz_f}{d\omega}\left(\frac{dt_f}{d\omega}\right)^{-1} = c\left[1+c\left(\frac{\partial\omega}{\partial f_l}\right)\left(\frac{\partial^2\phi_l^{q,\ell}}{\partial\omega^2}\right)\right]^{-1}. \quad (20)$$

The focal velocity can be tuned by adjusting the properties of the plasma lens, the mode numbers, or the initial spectral phase of the laser pulse $\phi_I(\omega)$.

Up to this point, the analysis has considered a laser pulse with an arbitrary frequency spectrum. For the remainder, it is convenient to consider a laser pulse characterized by a "central" frequency ω_0 and a spectral width $\tau^{-1} \ll \omega_0$. When the conditions $|R_I| \gg Z_I \gg Z_m$ and $Z_l \gg |R_l|$ are satisfied (see Appendix A), the spectral phase at the exit of the plasma lens is independent of q and ℓ:

$$\phi_l^{q,\ell}(\omega) \approx \phi_I(\omega) - \frac{\omega_{p0}^2}{2c\omega}L_p \equiv \phi_l(\omega), \quad (21)$$

where constant phase terms have been dropped. Because the focal velocity depends on $\partial_\omega^2\phi_l$, an initial second-order spectral phase

$$\phi_I(\omega) = \tfrac{1}{2}\phi_2(\omega-\omega_0)^2 \quad (22)$$

is the simplest phase that provides control over the velocity. This is equivalent to chirping the laser pulse. More specifically, one can write $\phi_2 = \hat{\eta}\tau^2/2$, where the chirp parameter $\hat{\eta}$ quantifies the temporal elongation of the pulse.

The plasma contribution to the spectral phase [Eq. (21)] can be compensated by the initial spectral phase ϕ_I. To second order in $\omega - \omega_0$,

$$\phi_l(\omega) \approx \frac{1}{4}\left(\hat{\eta} - \frac{2\omega_{p0}^2L_p}{c\omega_0^3\tau^2}\right)\tau^2(\omega-\omega_0)^2, \quad (23)$$

where constant and linear phase terms have been dropped (the latter would only result in an overall temporal delay). Thus, setting the chirp parameter $\hat{\eta} = \eta + 2\omega_{p0}^2L_p/c\omega_0^3\tau^2$ compensates the second-order phase acquired in the plasma lens and results in a spectral phase determined solely by η. A higher-order phase could also be compensated by introducing higher-order terms in ϕ_I. However, for the cases considered here, the second-order phase is already small: $2\omega_{p0}^2L_p/c\tau^2\omega_0^3 \ll 1$.

With the compensated spectral phase [Eq. (23)], the chromatic focusing of the chirped pulse results in the focal velocity

$$\frac{v_f(\omega)}{c} = \left[1+\frac{\eta\left(\frac{c\tau}{w_m}\right)^2\frac{Z_m}{L_p}\sin^2\left(\frac{L_p}{Z_m}\right)}{1+\frac{Z_m}{2L_p}\sin\left(\frac{2L_p}{Z_m}\right)}\right]^{-1}. \quad (24)$$

The focal velocity depends on frequency through the matched Rayleigh range $Z_m = \omega w_m^2/2c$. To first approximation, this dependence can be ignored, and ω can be replaced by ω_0 because $\omega_0\tau \ll 1$. As a result, the focal velocity is nearly constant throughout the focal range L_f.

For large values of the chirp parameter ($|\eta| \gg 1$), the stationary phase approximation can be used in Eq. (1) to find the

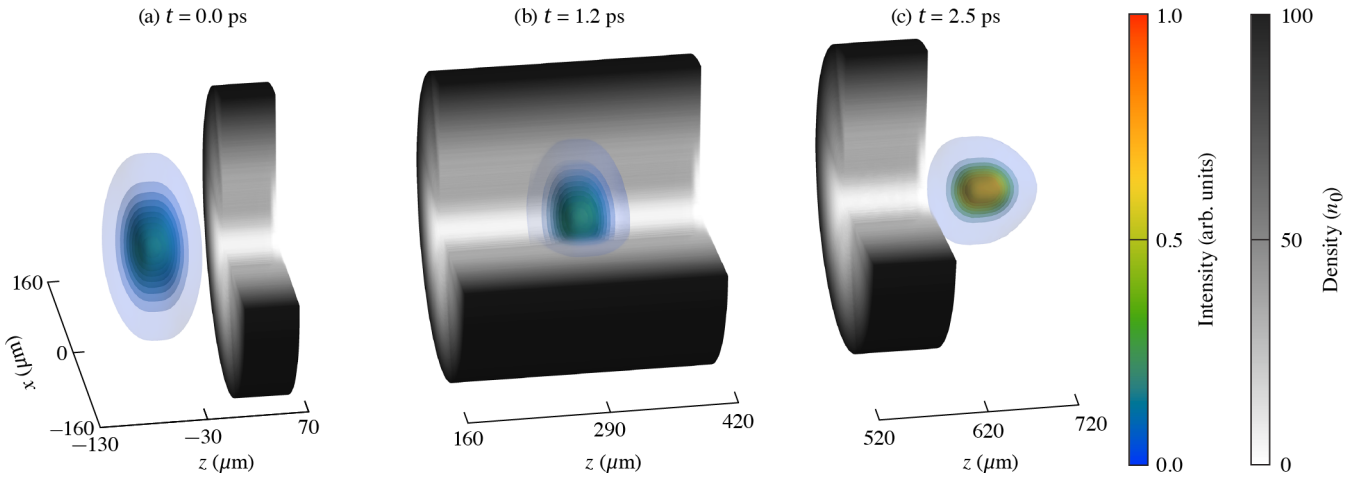

FIG. 2. Density contours of the plasma lens (gray scale) and intensity contours (color scale) of a laser pulse traversing the plasma lens. For this design, the plasma lens is thick, and the spot size of the laser pulse decreases appreciably from the entrance to the exit of the lens (left to right). The incident laser pulse has a normalized amplitude of $a_I = 0.5$ and a chirp parameter of $\eta = -5$. All other parameters can be found in Table I.

electric field of the laser pulse in the time domain:

$$E(\mathbf{x}, \xi) \approx \frac{\mathrm{sgn}(\eta)}{(4\pi|\eta|\tau^2)^{1/2}} \tilde{E}(\mathbf{x}, \omega_s) e^{-i(\omega_s \xi - \frac{\pi}{4})} + \text{c.c.}, \quad (25)$$

where $\omega_s = \omega_0 + 2\xi/\eta\tau^2$. The time-domain envelope of the laser pulse $\tilde{E}(\mathbf{x}, \omega_s)$ is given by Eq. (2) with ω replaced by ω_s. Using Eqs. (6) and (10) and the replacement $\omega \to \omega_s$ in Eq. (12) yields the temporal profile of the moving focus within the focal range:

$$I_f \propto \frac{w_I^2 A_I^2}{w^2(z)} \approx \frac{w_I^2 A_I^2}{w_f^2} \left[1 + \left(\frac{t - z/v_f - \zeta_0}{\tau_f} \right)^2 \right]^{-1}, \quad (26)$$

where

$$\tau_f = \left| \frac{c - v_f}{c v_f} \right| \frac{\omega_0 w_f^2}{2c} \quad (27)$$

is the duration of the intensity peak and $\zeta_0 = (v_f - c)[L_p + f_l(\omega_0)]/cv_f$ is the focal time with respect to the coordinate $\zeta = t - z/v_f$ for $\omega = \omega_0$. The maximum value of the moving intensity peak will be approximately constant within the focal range if the spectral amplitude $A_I(\omega)$ is constant for $\omega_{\min} \leqslant \omega \leqslant \omega_{\max}$.

IV. DESIGN CONSIDERATIONS

A distinguishing property of a flying focus is that the peak intensity can be maintained over a distance greater than the Rayleigh range of the focused spot. To take advantage of this property and to ensure that the focal trajectory can be clearly identified, the plasma lens should be designed so that

$$L_f > \frac{\omega_0 w_f^2}{2c}. \quad (28)$$

In addition, the parameters for the plasma lens should be chosen to avoid resonance absorption and mitigate parametric instabilities. This can be accomplished by keeping the maximum density experienced by the pulse $n_{\max} \sim n_2 w_I^2$ well below the critical density $n_{\text{cr}} = m_e \varepsilon_0 \omega_0^2 / e^2$. Equation (28) can be re-expressed in terms of these densities and the length of the plasma lens as follows:

$$\left(\frac{\Delta\omega L_p}{2c} \right) \left(\frac{n_{\max}}{n_{\text{cr}}} \right) > 1, \quad (29)$$

where $\Delta\omega \equiv \omega_{\max} - \omega_{\min}$ is the total bandwidth of the laser pulse and $L_f \approx \Delta\omega \partial_\omega f_l$ has been used. Preventing instabilities like two-plasmon decay and absolute stimulated Raman scattering requires $n_{\max}/n_{\text{cr}} \lesssim 1/4$. Thus, for a fixed bandwidth $\Delta\omega$, the length of the focal region relative to the Rayleigh range is determined solely by L_p. Note, however, that (i) L_p can only be increased up to $\pi Z_m/2$ before the plasma lens becomes a defocusing lens [see Eq. (16)], and (ii) a longer plasma lens may exacerbate instabilities like stimulated Raman forward scattering.

With these considerations in mind, a plasma lens was designed to produce flying foci over a range $L_f = \omega_0 w_f^2/c$. The parameters, displayed in Table I, were motivated by commercially available Ti:sapphire laser systems and experimentally demonstrated plasma channels [27,53–56]. The rightmost column of the table provides the parameters in normalized units to facilitate scaling the results presented here to other laser wavelengths or plasma densities. For this design, $L_p \approx Z_m$. As a result, the plasma lens is thick, and the spot size evolves significantly within the lens (Fig. 2).

V. SIMULATION RESULTS

The model presented in the previous sections illustrates the salient phenomena underlying a plasma-lens-based flying focus. Nevertheless, the model neglects nonparaxial and nonlinear propagation effects, such as stimulated Raman scattering, self-focusing, ponderomotively driven density modifications, and the increase in the effective electron mass due to relativistic motion. This section presents the results of quasi-three-dimensional particle-in-cell (PIC) simulations that include these effects (see Appendix B for details).

TABLE I. Laser pulse and plasma lens parameters used in the simulations. In the rightmost column, space, time, and density are normalized by c/ω_0, $1/\omega_0$, and $n_{cr} = m_e\varepsilon_0\omega_0^2/e^2$. The vacuum wavelength $\lambda_0 = 2\pi c/\omega_0$. The chirp parameter η was varied to change the focal velocity. For these parameters, the pulse takes about 3.4 ps to travel from the entrance of the plasma lens to the initial focal point at $z = L_p + f_l(\omega_0)$.

Pulse parameters	Value	Normalized
λ_0	800 nm	2π
ω_0	2.4×10^{15} rad/s	1
$\Delta\omega$ (FWHM)	1.4×10^{14} rad/s	0.061
τ	21 fs	51
R_I	∞	∞
w_I	60 μm	470
Plasma lens parameters	**Value**	**Normalized**
n_0	1×10^{18} cm^{-3}	5.7×10^{-4}
w_m	12.5 μm	98
L_p	0.61 mm	4.8×10^3
$f_l(\omega_0)$	0.4 mm	3.1×10^3
$w_f(\omega_0)$	3.1 μm	24
L_f	77 μm	604
$f/\#$	6.1	6.1

For incident intensities up to $I_I = 5.4 \times 10^{17}$ W/cm^2, the simulations demonstrate that the plasma-lens-based flying focus works as designed, validating the model. For incident intensities $I_I \gtrsim 2 \times 10^{18}$ W/cm^2, the simulations show that nonlinear effects disrupt the focusing of the plasma lens and formation of a flying focus. Notably, these intensities correspond to normalized amplitudes $a_I \equiv eE_I/m_e c\omega_0$ equal to 0.5 and 1.0, respectively, where $E_I = \max[E(\mathbf{x}_\perp, z = 0, \xi)]$, which straddle the transition from nonrelativistic to relativistic electron motion.

The incident laser pulse was initialized in the frequency domain as in Eq. (2) with a transverse Gaussian profile ($q = \ell = 0$). The initial spectral amplitude had the super-Gaussian profile

$$A_I(\omega) = \exp\left\{-\left[\tfrac{1}{2}\tau(\omega - \omega_0)\right]^4\right\}, \tag{30}$$

with a corresponding full width at half maximum (FWHM) $\Delta\omega = (4/\tau)[\ln(2)/2]^{1/4}$. The relatively flat spectral amplitude was chosen to ensure a near-constant peak intensity within the focal region. The initial spectral phase was specified as in Eq. (22) with $\phi_2 = \eta\tau^2/2$. The on-axis plasma density n_0 was low enough that the plasma contributed a negligible second-order phase. All other parameters can be found in Table I.

Figure 3 demonstrates that a plasma lens can produce a moving intensity peak with a predesigned velocity v_f. The panels show the on-axis ($r = 0$) spatiotemporal profile of the intensity peak as it traverses the focal range for four different chirp values. In each case, the moving focus has a near-constant velocity as predicted by Eq. (24) (white dashed lines). Note that with respect to the moving-frame coordinate $\xi = t - z/c$, the intensity peak follows the trajectory $z = cv_f\xi/(c - v_f)$. Beyond the focal range, the pulse diffracts, causing the moving intensity peak to gradually fade away.

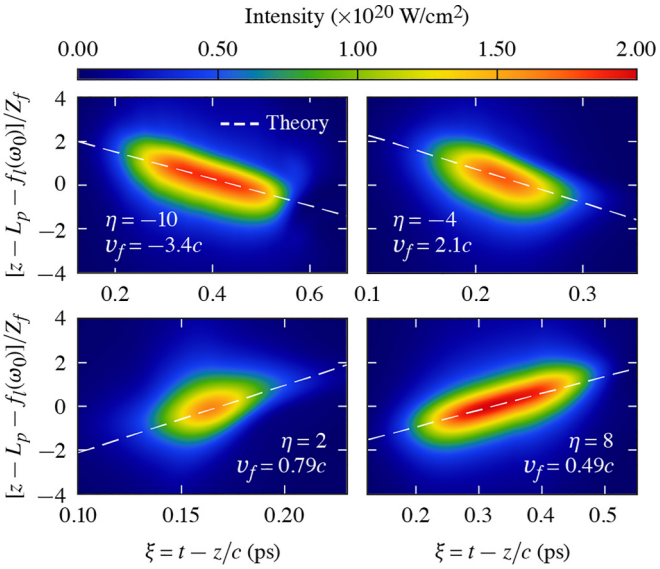

FIG. 3. Spatiotemporal profiles of the moving focus within the focal range for different focal velocities v_f (or chirps η) at $r = 0$. The intensity peak has a near-constant velocity and a maximum intensity that is consistent with the theory. In each case, the incident laser pulse had a normalized amplitude of $a_I = 0.5$. The distance from the nominal focus $f_l(\omega_0)$ is normalized to the Rayleigh range of the focused spot at the central frequency $Z_f \equiv cw_f^2/2\omega_0$.

Figure 4 compares the focal velocities calculated from the theory and simulations for all simulated chirp values. For focal velocities ranging from negative to positive superluminal, the two are in excellent agreement. Slight discrepancies can be observed for small values of the chirp parameter ($|\eta| \leqslant 2$). At these chirps, the effective duration of the moving focus τ_f [Eq. (27)] becomes larger than the duration of the laser pulse. In addition, the temporal profile of the laser pulse begins to approach the transform-limited profile, which no longer resembles the spectral amplitude (i.e., the stationary phase approximation breaks down). The combination of these effects makes it difficult to discern the intensity peak of the moving focus from the inherent intensity peak of the temporal profile.

In Fig. 3, the incident laser pulses had an amplitude of $a_I = 0.5$, corresponding to an intensity of $I_I = 5.4 \times 10^{17}$ W/cm^2. For the larger chirp values, the peak intensity at focus is consistent with Eqs. (6) and (10): $I_f = (w_I/w_f)^2 I_I = 2 \times 10^{20}$ W/cm^2. The slightly lower intensity when $\eta = 2$ results from modifications to the temporal profile not captured within the stationary phase approximation as discussed above (i.e., the temporal profile is approaching its transform limit).

As the incident amplitude of the laser pulse is pushed beyond $a_I = 0.5$, nonlinear propagation within the plasma lens and the nonlinear plasma response begin to disrupt the formation of a flying focus. Figure 5 shows the on-axis intensity profile at $z = L_p + f_l(\omega_0)$ normalized to the maximum of the incident intensity for $a_I = 0.1$, 0.5, and 1.0, and three stretched pulse durations (chirp values). For the shorter pulse durations ($\eta = -4$ and -8), the $a_I = 0.1$ and $a_I = 0.5$ pro-

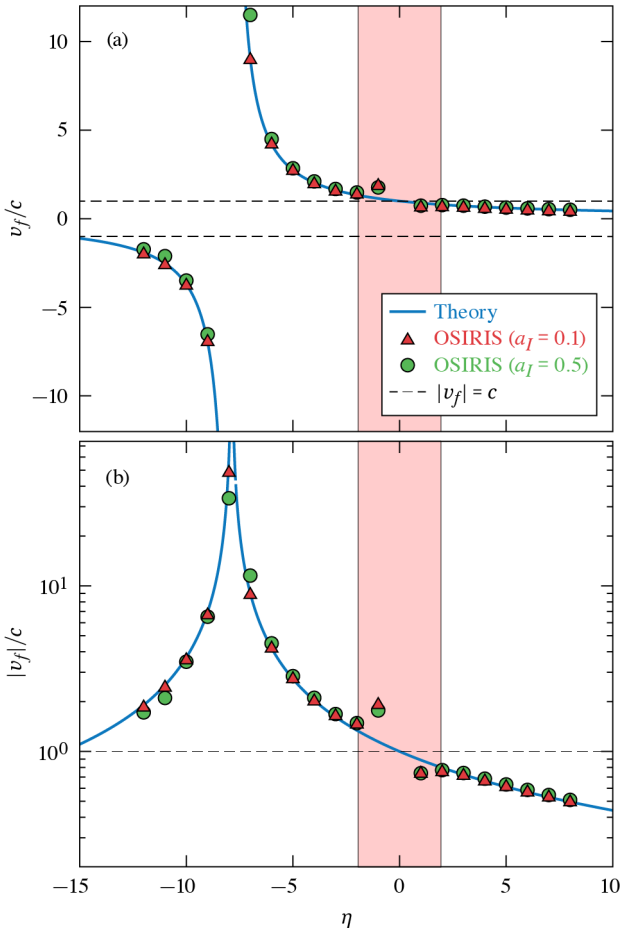

FIG. 4. Comparison of the focal velocities predicted by the thick lens theory [Eq. (24)] and the PIC simulations as a function of the chirp parameter η. The theory and simulations are in excellent agreement when the effective duration τ_f is larger than the stretched pulse duration (outside the red shaded area).

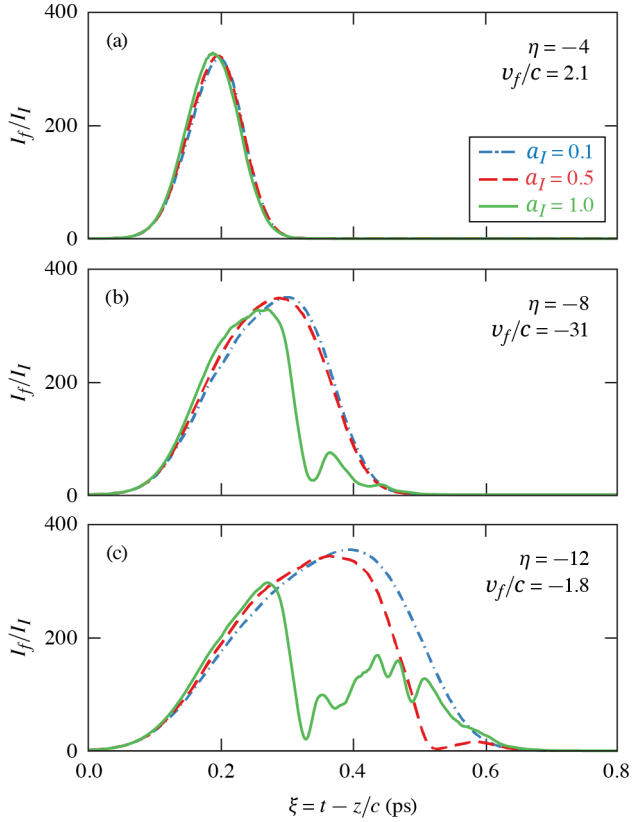

FIG. 5. Temporal profiles of the on-axis intensity at the nominal focal point $z = L_p + f_l(\omega_0)$ for three different focal velocities (or chirps η) and incident amplitudes a_I. In all cases, the intensity is normalized to the incident intensity I_I. Pulses with longer durations and larger amplitudes are more susceptible to modifications due to nonlinear propagation and plasma evolution.

files are nearly identical, indicating that nonlinear effects have not modified the plasma lens focusing. For the longest pulse duration ($\eta = -12$), the profile of the $a_I = 0.1$ pulse remains unmodified, while the back half of the $a_I = 0.5$ pulse has become distorted. When $a_I = 1$, this distortion occurs earlier within the pulse and is already apparent at the intermediate duration $\eta = -8$. At the longest pulse duration ($\eta = -12$), the entire back half of the pulse has deteriorated.

The pulse-length dependence of the distortion suggests that it results from the feedback between the ponderomotively modified electron density profile and the laser pulse. Mitigating nonlinear modifications to the pulse requires either lowering the incident amplitude or shortening the stretched pulse duration. To shorten the duration for a fixed focal spot size (f-number) and focal velocity [Eqs. (17) and (24)], one can use the scalings $\tau \to \chi\tau$, $\Delta\omega \to \chi^{-1}\Delta\omega$, $w_m \to \chi w_m$, $L_p \to \chi^2 L_p$, $w_I \to \chi^2 w_I$, and $n_{\max} \to n_{\max}$. With these scalings, the right-hand side of Eq. (29) $\to \chi(\Delta\omega L_p n_{\max})/(2cn_{\rm cr})$. This scaling shows that decreasing the duration ($\chi < 1$) makes it more difficult to satisfy Eq. (29). As a result, lowering the amplitude may be the preferable option for mitigating nonlinear modifications to the pulse.

VI. CONCLUSIONS AND PROSPECTS

Plasma optics allow for spatiotemporal control at orders of magnitude higher intensities than conventional optics. In the specific case considered here, a chirped laser pulse focused by a plasma lens exhibits a dynamic or "flying" focus that moves independently of the group or phase velocities. By adjusting the chirp, the velocity of the moving focus can be varied from sub to superluminal in either the forward or backward directions. The plasma lens operates as designed up to near-relativistic intensities ($I \approx 6 \times 10^{17}$ W/cm^2) and could be formed by adapting the experimental techniques used to produce plasma channels [54–56].

The parameters of the plasma lens considered were motivated by experimentally demonstrated plasma channels [27,53–56]. With these parameters, the incident intensity $I_I = 5.4 \times 10^{17}$ W/cm^2 resulted in a focused intensity of $I_f = 2.0 \times 10^{20}$ W/cm^2. The focused intensity can be increased or decreased by scaling the parameters of the plasma lens. For a fixed incident intensity and focused spot size (or f-number), the scalings $w_I \to \chi w_I$, $w_m \to \chi^{1/2} w_m$, $L_p \to \chi L_p$, and $f_l \to \chi f_l$ result in a focused intensity $I_f \to \chi^2 I_f$. As an example, achieving a plasma-lens-based flying focus with a world-record intensity of $I_f = 1 \times 10^{23}$ W/cm^2 [57] would require a plasma lens with a maximum radius of

$r_{\max} \sim w_I \sim 1.2$ mm and a length of $L_p \sim 1.2$ cm. This would require further advances in techniques for plasma channel formation.

As an alternative to plasma channels, a plasma lens can also be created by using the interference of two laser beams to structure the plasma density through ionization or ponderomotive forces [43]. These holographic plasma lenses operate like a diffractive lens and are inherently chromatic. A chirped laser pulse focused by such a plasma lens would also produce a flying focus. Future work will consider this alternative and explore other plasma configurations that can controllably modify the space-time structure of laser pulses. For instance, a plasma-based version of the ultrafast flying focus [8] or the flying focus X [11] could allow for arbitrary focal velocities and an ultrashort-duration intensity peak that travels distances much greater than a Rayleigh range.

ACKNOWLEDGMENTS

The authors would like to thank J. Vieira, T. T. Simpson, D. Ramsey, and D. H. Froula for productive discussions. The work of D.L. and A.G.R.T. is supported by the National Science Foundation under Award No. NSF-2108075 and the Office of Fusion Energy Sciences under Award No. DE-SC0022109. The work of J.R.P. and W.B.M. is supported by the LLE under Subcontract No. SUB00000211/GR531765, the National Science Foundation under Award No. NSF-2108970, and the Department of Energy National Nuclear Security Administration under Award No. DE-NA0004131. The work of K.G.M. and J.P.P. is supported by the Office of Fusion Energy Sciences under Award No. DE-SC0021057, the Department of Energy National Nuclear Security Administration under Award No. DE-NA0004144, the University of Rochester, and the New York State Energy Research and Development Authority.

APPENDIX A: OPERATING REGIME

This Appendix justifies the conditions $|R_I| \gg Z_I \gg Z_m$ and $Z_l \gg |R_l|$, which were used to simplify the equations derived in Secs. II and III. In any situation of interest, a plasma lens would be located far from an initial optical assembly. Suppose then that the laser pulse incident on the plasma lens was originally collimated and subsequently focused by a conventional lens with a focal length $f_I \approx |R_I|$ located at $z = -z_0 < 0$. At the entrance to the plasma lens, the spot size would be

$$w_I \approx w_0 \left[\left(\frac{\Delta}{f_I} \right)^2 + \left(\frac{w_D}{w_0} \right)^2 \right]^{1/2}, \tag{A1}$$

where w_0 is the spot size incident on the conventional lens, $\Delta \equiv |f_I - z_0| \ll f_I$ is the distance between the conventional focus and the entrance to the plasma lens, and $w_D = 2cf_I/\omega w_0$ is the diffraction-limited spot size. If the entrance to the plasma lens is located within the confocal region of the conventional lens, i.e., $\Delta \leqslant \omega w_D^2/2c$, then $w_I \approx w_D$. As a result, $|R_I|/Z_I \approx f_I/Z_I \approx w_0/w_D$. For the lenses of interest $w_0 \gg w_D$, such that $|R_I| \gg Z_I$. If the plasma lens is outside of the confocal region, i.e., $\Delta > \omega w_D^2/2c$, then $w_I \approx w_0\Delta/f_I$. In this case, $|R_I|/Z_I \approx f_I/Z_I \approx (w_D/w_0)(f_I/\Delta)^2$, which easily satisfies the first condition when the plasma lens is far from the conventional lens: $\Delta \ll (w_D/w_0)^{1/2} f_I$.

The condition $Z_I \gg Z_m$ is equivalent to $w_I^2/w_m^2 \gg 1$. When $|R_I|/Z_I \gg 1$, the spot size of the laser pulse can oscillate between w_I and w_m^2/w_I, depending on the length of the plasma lens [Eq. (8)]. A ratio $w_I/w_m > 1$ ensures that the laser pulse exits the plasma lens with a smaller spot than it entered with. Perhaps more importantly, the radius of curvature can oscillate in the plasma lens [Eq. (9)]. These oscillations can result in unintended defocusing of the laser pulse. When $R_I < 0$ (e.g., due to preliminary focusing by a conventional lens), $w_I > w_m$ ensures that the laser pulse accumulates a stronger focusing phase over the initial length of the plasma lens. This initial length L_i and the ultimate strength of the focusing phase reach their maximum in the limit $w_I^2/w_m^2 \to \infty$. More specifically, $L_i \to \pi Z_m/2$ and $R \to 0$ from below. Thus, operating in a regime where $w_I^2/w_m^2 \gg 1$ provides a larger range of available focusing powers and a larger margin on the length of the plasma before one needs to worry about a sign reversal in the curvature phase. Finally, for any focusing plasma lens of use, the focused spot size w_f will be much smaller than the spot size at the exit of the lens w_l, such that $Z_l/|R_l| = \omega w_l^2/2c|R_l| \approx w_l/w_f \gg 1$.

APPENDIX B: SIMULATION DETAILS

The simulations presented in this work were performed using OSIRIS with the moving-window and quasi-three-dimensional capabilities [58–60]. The transverse domain consisted of two azimuthal modes and 600 cells over 240 μm in the radial direction. The longitudinal domain was scaled with the chirp to contain the stretched duration of the laser pulse. The minimum and maximum numbers of longitudinal cells were 3200 and 9600, corresponding to lengths of 80 and 240 μm. The longitudinal resolution was fixed at $\Delta\xi \sim 25$ nm to maintain 30 grid points per the shortest wavelength in the pulse.

The electromagnetic fields and particle motion were evolved with the dual solver, which ensures accurate dispersion of the waves and eliminates time-staggering errors in the Lorentz force [61]. To accomplish this, the dual solver employed finite-difference operators with 16 coefficients. A 0.083-fs time step was set to satisfy the Courant condition, and the simulation duration was ~6 ps. Open boundary conditions were applied for both the fields and particles. In the region occupied by the plasma lens, the ions were fixed, and 32 particles per cell were used for the electrons. The plasma lens had 10-μm density ramps at its entrance and exit.

[1] S. Longhi, Spatial-temporal Gauss-Laguerre waves in dispersive media, Phys. Rev. E **68**, 066612 (2003).

[2] H. E. Kondakci and A. F. Abouraddy, Diffraction-free space–time light sheets, Nat. Photon. **11**, 733 (2017).

[3] A. Sainte-Marie, O. Gobert, and F. Quéré, Controlling the velocity of ultrashort light pulses in vacuum through spatio-temporal couplings, Optica **4**, 1298 (2017).

[4] D. H. Froula, D. Turnbull, A. S. Davies, T. J. Kessler, D. Haberberger, J. P. Palastro, S.-W. Bahk, I. A. Begishev, R. Boni, S. Bucht, J. Katz, and J. L. Shaw, Spatiotemporal control of laser intensity, Nat. Photon. **12**, 262 (2018).

[5] H. E. Kondakci and A. F. Abouraddy, Optical space-time wave packets having arbitrary group velocities in free space, Nat. Commun. **10**, 929 (2019).

[6] Z. Li and J. Kawanaka, Optical wave-packet with nearly-programmable group velocities, Commun. Phys. **3**, 211 (2020).

[7] Z. Li and J. Kawanaka, Velocity and acceleration freely tunable straight-line propagation light bullet, Sci. Rep. **10**, 11481 (2020).

[8] J. P. Palastro, J. L. Shaw, P. Franke, D. Ramsey, T. T. Simpson, and D. H. Froula, Dephasingless laser wakefield acceleration, Phys. Rev. Lett. **124**, 134802 (2020).

[9] S. W. Jolly, O. Gobert, A. Jeandet, and F. Quéré, Controlling the velocity of a femtosecond laser pulse using refractive lenses, Opt. Express **28**, 4888 (2020).

[10] C. Caizergues, S. Smartsev, V. Malka, and C. Thaury, Phase-locked laser-wakefield electron acceleration, Nat. Photon. **14**, 475 (2020).

[11] T. T. Simpson, D. Ramsey, P. Franke, K. Weichman, M. V. Ambat, D. Turnbull, D. H. Froula, and J. P. Palastro, Spatiotemporal control of laser intensity through cross-phase modulation, Opt. Express **30**, 9878 (2022).

[12] I. M. Besieris and P. Saari, Autofocusing luminal and superluminal spatiotemporally localized waves, J. Opt. Soc. Am. A **39**, 1449 (2022).

[13] M. Yessenov, J. Free, Z. Chen, E. G. Johnson, M. P. J. Lavery, M. A. Alonso, and A. F. Abouraddy, Space-time wave packets localized in all dimensions, Nat. Commun. **13**, 4573 (2022).

[14] J. R. Pierce, J. P. Palastro, F. Li, B. Malaca, D. Ramsey, J. Vieira, K. Weichman, and W. B. Mori, Arbitrarily structured laser pulses, Phys. Rev. Res. **5**, 013085 (2023).

[15] D. Ramsey, A. Di Piazza, M. Formanek, P. Franke, D. H. Froula, B. Malaca, W. B. Mori, J. R. Pierce, T. T. Simpson, J. Vieira, M. Vranic, K. Weichman, and J. P. Palastro, Exact solutions for the electromagnetic fields of a flying focus, Phys. Rev. A **107**, 013513 (2023).

[16] Z. Liang, Y. Liu, Y. Luo, H. Chen, and D. Deng, Space-time wave packets with both arbitrary transverse and longitudinal accelerations, Opt. Lett. **48**, 2543 (2023).

[17] M. V. Ambat, J. L. Shaw, J. J. Pigeon, K. G. Miller, T. T. Simpson, D. H. Froula, and J. P. Palastro, Programmable-trajectory ultrafast flying focus pulses, Opt. Express **31**, 31354 (2023).

[18] J. J. Pigeon, P. Franke, M. Lim Pac Chong, J. Katz, R. Boni, C. Dorrer, J. P. Palastro, and D. H. Froula, Ultrabroadband flying-focus using an axiparabola-echelon pair, Opt. Express **32**, 576 (2024).

[19] D. Turnbull, S. Bucht, A. Davies, D. Haberberger, T. Kessler, J. L. Shaw, and D. H. Froula, Raman amplification with a flying focus, Phys. Rev. Lett. **120**, 024801 (2018).

[20] J. P. Palastro, D. Turnbull, S.-W. Bahk, R. K. Follett, J. L. Shaw, D. Haberberger, J. Bromage, and D. H. Froula, Ionization waves of arbitrary velocity driven by a flying focus, Phys. Rev. A **97**, 033835 (2018).

[21] A. J. Howard, D. Turnbull, A. S. Davies, P. Franke, D. H. Froula, and J. P. Palastro, Photon acceleration in a flying focus, Phys. Rev. Lett. **123**, 124801 (2019).

[22] A. Di Piazza, Unveiling the transverse formation length of nonlinear Compton scattering, Phys. Rev. A **103**, 012215 (2021).

[23] D. Ramsey, B. Malaca, A. Di Piazza, M. Formanek, P. Franke, D. H. Froula, M. Pardal, T. T. Simpson, J. Vieira, K. Weichman, and J. P. Palastro, Nonlinear Thomson scattering with ponderomotive control, Phys. Rev. E **105**, 065201 (2022).

[24] M. Formanek, D. Ramsey, J. P. Palastro, and A. Di Piazza, Radiation reaction enhancement in flying focus pulses, Phys. Rev. A **105**, L020203 (2022).

[25] A. Kabacinski, E. Oliva, F. Tissandier, J. Gautier, M. Kozlová, J.-P. Goddet, I. A. Andriyash, C. Thaury, P. Zeitoun, and S. Sebban, Spatio-temporal couplings for controlling group velocity in longitudinally pumped seeded soft x-ray lasers, Nat. Photon. **17**, 354 (2023).

[26] T. T. Simpson, J. J. Pigeon, M. V. Ambat, K. G. Miller, D. Ramsey, K. Weichman, D. H. Froula, and J. P. Palastro, Spatiotemporal control of two-color terahertz generation, Phys. Rev. Res. **6**, 013041 (2024).

[27] C. G. Durfee and H. M. Milchberg, Light pipe for high intensity laser pulses, Phys. Rev. Lett. **71**, 2409 (1993).

[28] V. M. Malkin, G. Shvets, and N. J. Fisch, Fast compression of laser beams to highly overcritical powers, Phys. Rev. Lett. **82**, 4448 (1999).

[29] Y. Ping, I. Geltner, N. J. Fisch, G. Shvets, and S. Suckewer, Demonstration of ultrashort laser pulse amplification in plasmas by a counterpropagating pumping beam, Phys. Rev. E **62**, R4532 (2000).

[30] R. F. Hubbard, B. Hafizi, A. Ting, D. Kaganovich, P. Sprangle, and A. Zigler, High intensity focusing of laser pulses using a short plasma channel lens, Phys. Plasmas **9**, 1431 (2002).

[31] G. Doumy, F. Quéré, O. Gobert, M. Perdrix, P. Martin, P. Audebert, J. C. Gauthier, J.-P. Geindre, and T. Wittmann, Complete characterization of a plasma mirror for the production of high-contrast ultraintense laser pulses, Phys. Rev. E **69**, 026402 (2004).

[32] A. Lévy, T. Ceccotti, P. D'Oliveira, F. Réau, M. Perdrix, F. Quéré, P. Monot, M. Bougeard, H. Lagadec, P. Martin, J.-P. Geindre, and P. Audebert, Double plasma mirror for ultrahigh temporal contrast ultraintense laser pulses, Opt. Lett. **32**, 310 (2007).

[33] Y. Katzir, S. Eisenmann, Y. Ferber, A. Zigler, and R. F. Hubbard, A plasma microlens for ultrashort high power lasers, Appl. Phys. Lett. **95**, 031101 (2009).

[34] M. Nakatsutsumi, A. Kon, S. Buffechoux, P. Audebert, J. Fuchs, and R. Kodama, Fast focusing of short-pulse lasers by innovative plasma optics toward extreme intensity, Opt. Lett. **35**, 2314 (2010).

[35] J. P. Palastro, D. Gordon, B. Hafizi, L. A. Johnson, J. Peñano, R. F. Hubbard, M. Helle, and D. Kaganovich, Plasma lenses for ultrashort multi-petawatt laser pulses, Phys. Plasmas **22**, 123101 (2015).

[36] D. Turnbull, P. Michel, T. Chapman, E. Tubman, B. B. Pollock, C. Y. Chen, C. Goyon, J. S. Ross, L. Divol, N. Woolsey, and

J. D. Moody, High power dynamic polarization control using plasma photonics, Phys. Rev. Lett. **116**, 205001 (2016).

[37] G. Lehmann and K. H. Spatschek, Transient plasma photonic crystals for high-power lasers, Phys. Rev. Lett. **116**, 225002 (2016).

[38] A. Leblanc, A. Denoeud, L. Chopineau, G. Mennerat, P. Martin, and F. Quéré, Plasma holograms for ultrahigh-intensity optics, Nat. Phys. **13**, 440 (2017).

[39] K. Qu, Q. Jia, and N. J. Fisch, Plasma q-plate for generation and manipulation of intense optical vortices, Phys. Rev. E **96**, 053207 (2017).

[40] G. Vieux, S. Cipiccia, D. W. Grant, N. Lemos, P. Grant, C. Ciocarlan, B. Ersfeld, M. S. Hur, P. Lepipas, G. G. Manahan, G. Raj, D. Reboredo Gil, A. Subiel, G. H. Welsh, S. M. Wiggins, S. R. Yoffe, J. P. Farmer, C. Aniculaesei, E. Brunetti, X. Yang *et al.*, An ultra-high gain and efficient amplifier based on Raman amplification in plasma, Sci. Rep. **7**, 2399 (2017).

[41] R. K. Kirkwood, D. P. Turnbull, T. Chapman, S. C. Wilks, M. D. Rosen, R. A. London, L. A. Pickworth, W. H. Dunlop, J. D. Moody, D. J. Strozzi, P. A. Michel, L. Divol, O. L. Landen, B. J. MacGowan, B. M. Van Wonterghem, K. B. Fournier, and B. E. Blue, Plasma-based beam combiner for very high fluence and energy, Nat. Phys. **14**, 80 (2018).

[42] H. Peng, C. Riconda, S. Weber, C. T. Zhou, and S. C. Ruan, Frequency conversion of lasers in a dynamic plasma grating, Phys. Rev. Appl. **15**, 054053 (2021).

[43] M. R. Edwards, V. R. Munirov, A. Singh, N. M. Fasano, E. Kur, N. Lemos, J. M. Mikhailova, J. S. Wurtele, and P. Michel, Holographic plasma lenses, Phys. Rev. Lett. **128**, 065003 (2022).

[44] M. R. Edwards and P. Michel, Plasma transmission gratings for compression of high-intensity laser pulses, Phys. Rev. Appl. **18**, 024026 (2022).

[45] S. C. Wilks, J. M. Dawson, W. B. Mori, T. Katsouleas, and M. E. Jones, Photon accelerator, Phys. Rev. Lett. **62**, 2600 (1989).

[46] R. T. Sandberg and A. G. R. Thomas, Photon acceleration from optical to XUV, Phys. Rev. Lett. **130**, 085001 (2023).

[47] P. Michel, L. Divol, E. A. Williams, S. Weber, C. A. Thomas, D. A. Callahan, S. W. Haan, J. D. Salmonson, S. Dixit, D. E. Hinkel, M. J. Edwards, B. J. MacGowan, J. D. Lindl, S. H. Glenzer, and L. J. Suter, Tuning the implosion symmetry of icf targets via controlled crossed-beam energy transfer, Phys. Rev. Lett. **102**, 025004 (2009).

[48] S. H. Glenzer, B. J. MacGowan, P. Michel, N. B. Meezan, L. J. Suter, S. N. Dixit, J. L. Kline, G. A. Kyrala, D. K. Bradley, D. A. Callahan, E. L. Dewald, L. Divol, E. Dzenitis, M. J. Edwards, A. V. Hamza, C. A. Haynam, D. E. Hinkel, D. H. Kalantar, J. D. Kilkenny, O. L. Landen *et al.*, Symmetric inertial confinement fusion implosions at ultra-high laser energies, Science **327**, 1228 (2010).

[49] C. G. R. Geddes, C. Toth, J. van Tilborg, E. Esarey, C. B. Schroeder, D. Bruhwiler, C. Nieter, J. Cary, and W. P. Leemans, High-quality electron beams from a laser wakefield accelerator using plasma-channel guiding, Nature (London) **431**, 538 (2004).

[50] B. Miao, J. E. Shrock, L. Feder, R. C. Hollinger, J. Morrison, R. Nedbailo, A. Picksley, H. Song, S. Wang, J. J. Rocca, and H. M. Milchberg, Multi-gev electron bunches from an all-optical laser wakefield accelerator, Phys. Rev. X **12**, 031038 (2022).

[51] P. Franke, D. Ramsey, T. T. Simpson, D. Turnbull, D. H. Froula, and J. P. Palastro, Optical shock-enhanced self-photon acceleration, Phys. Rev. A **104**, 043520 (2021).

[52] M. Formanek, J. P. Palastro, D. Ramsey, S. Weber, and A. D. Piazza, Signatures of vacuum birefringence in low-power flying focus pulses, Phys. Rev. D **109**, 056009 (2024).

[53] C. G. Durfee, J. Lynch, and H. M. Milchberg, Development of a plasma waveguide for high-intensity laser pulses, Phys. Rev. E **51**, 2368 (1995).

[54] V. Kumarappan, K. Y. Kim, and H. M. Milchberg, Guiding of intense laser pulses in plasma waveguides produced from efficient, femtosecond end-pumped heating of clustered gases, Phys. Rev. Lett. **94**, 205004 (2005).

[55] D. H. Froula, L. Divol, P. Davis, J. P. Palastro, P. Michel, V. Leurent, S. H. Glenzer, B. B. Pollock, and G. Tynan, Magnetically controlled plasma waveguide for laser wakefield acceleration, Plasma Phys. Control. Fusion **51**, 024009 (2009).

[56] R. J. Shalloo, C. Arran, L. Corner, J. Holloway, J. Jonnerby, R. Walczak, H. M. Milchberg, and S. M. Hooker, Hydrodynamic optical-field-ionized plasma channels, Phys. Rev. E **97**, 053203 (2018).

[57] J. W. Yoon, Y. G. Kim, I. W. Choi, J. H. Sung, H. W. Lee, S. K. Lee, and C. H. Nam, Realization of laser intensity over 10^{23} W/cm^2, Optica **8**, 630 (2021).

[58] R. A. Fonseca, L. O. Silva, F. S. Tsung, V. K. Decyk, W. Lu, C. Ren, W. B. Mori, S. Deng, S. Lee, T. Katsouleas, and J. C. Adam, OSIRIS: A three-dimensional, fully relativistic particle in cell code for modeling plasma based accelerators, in *Computational Science–ICCS 2002: International Conference Amsterdam, The Netherlands, April 21–24, 2002, Proceedings, Part III*, edited by P. M. A. Sloot, A. G. Hoekstra, C. J. K. Tan, and J. J. Dongarra (Springer, Berlin, 2002), pp. 342–351.

[59] R. A. Fonseca, J. Vieira, F. Fiuza, A. Davidson, F. S. Tsung, W. B. Mori, and L. O. Silva, Exploiting multi-scale parallelism for large scale numerical modelling of laser wakefield accelerators, Plasma Phys. Control. Fusion **55**, 124011 (2013).

[60] A. Davidson, A. Tableman, W. An, F. Tsung, W. Lu, J. Vieira, R. Fonseca, L. Silva, and W. Mori, Implementation of a hybrid particle code with a PIC description in r-z and a gridless description in ϕ into OSIRIS, J. Comput. Phys. **281**, 1063 (2015).

[61] F. Li, K. G. Miller, X. Xu, F. S. Tsung, V. K. Decyk, W. An, R. A. Fonseca, and W. B. Mori, A new field solver for modeling of relativistic particle-laser interactions using the particle-in-cell algorithm, Comput. Phys. Commun. **258**, 107580 (2021).